Astronomy & Astrophysics manuscript no. master
March 3, 2017

High resolution near-IR spectroscopy of Arcturus and 10 Leo

Refining a near-IR iron line list

D. T. Andreasen[1,2], S. G. Sousa[1], E. Delgado Mena[1], N. C. Santos[1,2], T. Lebzelter[3], A. Mucciarelli[4,5], and J. Neal[1,2]

[1] Instituto de Astrofísica e Ciências do Espaço, Universidade do Porto, CAUP, Rua das Estrelas, 4150-762 Porto, Portugal, e-mail: daniel.andreasen@astro.up.pt
[2] Departamento de Física e Astronomia, Faculdade de Ciências, Universidade do Porto, Rua Campo Alegre, 4169-007 Porto, Portugal
[3] Institute for Astrophysics, University of Vienna, Türkenschanzstrasse 17, 1180 Vienna, Austria
[4] Dipartimento di Fisica e Astronomia, Universita' degli Studi di Bologna, Viale Berti Pichat, 6/2, 40126, Bologna, Italy
[5] INAF - Osservatorio Astronomico di Bologna, Via Ranzani 1, 40127, Bologna, Italy

Received ...; accepted ...

ABSTRACT

Context. Reliable stellar atmospheric parameters for FGK stars have been obtained mostly from methods that rely on high resolution and high signal-to-noise optical spectroscopy. The advent of a new generation of high resolution near-IR spectrographs opens the possibility of using classic spectroscopic methods with high resolution and high signal-to-noise in the NIR spectral window.
Aims. We aim to obtain precise and accurate atmospheric stellar parameters using high quality spectra of two K giant stars, Arcturus and 10 Leo.
Methods. Our spectroscopic analysis is based on the iron excitation and ionization balance done in LTE and a line list of Fe I and Fe II lines in the NIR domain. The line list is being refined from our previous study, allowing us to obtain more reliable parameters.
Results. We successfully obtain atmospheric parameters for two K giants in agreement with average literature values adopted.
Conclusions. With these results we are now extending the line list towards cooler stars, thus allowing us to explorer the M dwarf stars in the future, known to form Earth-like planets.

Key words. data reduction: high resolution spectra – stars individual: Arcturus – stars individual: 10 Leo

1. Introduction

Effective temperature ($T_{\rm eff}$), surface gravity ($\log g$), and metallicity ([M/H], where iron is normally used as a proxy) are fundamental atmospheric parameters necessary to characterise a single star, and to determine other indirectly fundamental parameters such as mass, radius, and age from stellar evolution models (see e.g. Girardi et al. 2000; Dotter et al. 2008; Baraffe et al. 2015). Precise and accurate stellar parameters are also essential in exoplanet searches. Planetary radius and mass are mainly found from transit lightcurve analysis and radial velocity analysis, respectively. The determination of the mass of the planet implies a knowledge of the stellar mass, while the measurement of the radius of the planet is dependent on our capability to derive the radius of the star (see e.g. Torres et al. 2008; Ammler-von Eiff et al. 2009; Torres et al. 2012).

The derivation of precise stellar atmospheric parameters is not a simple task. Different approaches often lead to discrepant results (see e.g. Torres et al. 2010; Lebzelter et al. 2012; Santos et al. 2013). Interferometry is usually considered an accurate method for deriving stellar radii (see e.g. Boyajian et al. 2012); however, it is only applicable for bright nearby stars. Asteroseismology, on the other hand, reveals the inner stellar structure by observing the stellar pulsations at the surface. From asteroseismology it is possible to measure the surface gravity and mean density, and therefore to calculate mass and radius with high precision (see e.g. Kjeldsen & Bedding 1995). However, for stars on the main sequence asteroseismic methods can typically only be applied to FG stars, since the oscillation modes of K and M dwarfs are likely too weak to be detected even with high precision spectroscopy or photometry. Moreover, the effective temperature is needed when applying asteroseismology in order to obtain the surface gravity and the mean density.

A crucial parameter for the indirect determination of stellar bulk properties is the $T_{\rm eff}$. In that respect, the infrared flux method (IRFM) has proven to be reliable for FGK dwarf and subgiant stars. For higher accuracy the IRFM needs a priori knowledge of the bolometric flux, reddening, surface gravity, and stellar metallicity (Blackwell & Shallis 1977; Ramírez & Meléndez 2005; Casagrande et al. 2010).

Finally, the use of high resolution spectroscopy along with stellar atmospheric models is an extensively tested method that allows the derivation of the fundamental parameters of a star (see e.g. Valenti & Fischer 2005; Santos et al. 2013). The procedure depends on the quality of the spectra, their resolution, and wavelength region. A fit to the overall spectrum can be applied for all spectral resolutions, but are often time consuming (see e.g. Recio-Blanco et al. 2006; Tsantaki et al. 2014). For resolutions higher than $\lambda/\Delta\lambda < 20\,000$ we can apply the equivalent width (EW) method (see e.g. Tsantaki et al. 2013; Andreasen et al. 2017, for details). However, while the latter approach is often faster than the synthetic fitting, it requires higher quality spectra, and the star to be slow rotating (below 10 km/s to 15 km/s).

Standard procedures are often used to derive stellar atmospheric parameters from high quality spectra in the optical (see e.g. Valenti & Fischer 2005; Sousa et al. 2008). With the advancement of high resolution near-infrared (NIR) instruments,

we will now be able to use a similar technique to that used in the optical part of the spectrum (see e.g. Meléndez & Barbuy 1999; Sousa et al. 2008; Tsantaki et al. 2013; Mucciarelli et al. 2013; Bensby et al. 2014). At the moment, the GIANO spectrograph installed at *Telescopio Nazionale Galileo* (TNG) is already available (Origlia et al. 2014), as is the *infrared Doppler instrument* (IRD) installed at the Subaru telescope (Kotani et al. 2014), *Calar Alto high-Resolution search for M dwarfs with Exoearths with Near-infrared and optical Échelle Spectrographs* (CARMENES) for the 3.5 m telescope at Calar Alto Observatory (Quirrenbach et al. 2014), and iShell at the *InfraRed Telescope Facility* (Rayner et al. 2012, 2016). Three new spectrographs are planned for the near future: 1) The *CRyogenic InfraRed Echelle Spectrograph Upgrade Project* (CRIRES+) at the *Very Large Telescope* (VLT) (Follert et al. 2014) with expected first light in 2017, 2) *un SpectroPolarimètre Infra-Rouge A Near-InfraRed Spectropolarimeter* (SPIRou) at *The Canada-France-Hawaii Telescope* (CFHT) (Delfosse et al. 2013; Artigau et al. 2014) with expected first light in 2017 as well, and 3) NIRPS at the ESO 3.6m telescope in La Silla (Conod et al. 2016). The spectral resolutions for these spectrographs range between 50 000 and 100 000.

With the advance of the next generation NIR spectrographs, we are still preparing the data analysis of stellar spectra, in particular how to get reliable atmospheric parameters (see e.g. Önehag et al. 2012; Lindgren et al. 2016; Andreasen et al. 2016). The analysis of stellar spectra is well understood for FGK stars in the optical part of the spectrum, however some work still needs to be done for the NIR part.

We continue our series of studies to explore the use of the NIR domain to derive stellar parameters for FGK and M stars. In particular, here we analyse the atlas of Arcturus and the spectrum of 10 Leo. For the analysis we use the iron line list presented in Andreasen et al. (2016) (referred to as Paper I). In Paper I we successfully tested our method on a slightly hotter star than the Sun, while in this work we aim to test the method on cooler stars. The strength of the NIR domain over the optical becomes clear when we move towards the cooler stars. Here we see less continuum depression and line blending due to in particular molecular features. Moreover, the cooler stars emit more light in the NIR domain than the optical, and with the lightest stars being intrinsically faint, we thus obtain the majority of the flux here.

2. Data

While the community is currently on the verge to access large amount of high resolution NIR spectra, the available spectra at the moment are sparse. We chose to use two stars cooler than the Sun since we used a hotter star (HD 20010) than the Sun in Paper I. The method used in Paper I and here is determining the iron abundances on a number of lines from their measured EWs. Then we impose ionization balance between Fe I and Fe II lines, and excitation balance for all Fe I lines, by changing the atmospheric parameters for the model atmosphere (Kurucz 1993, is used here).

We have used the atlas of Arcturus (acquired at Kitt Peak National Observatory using the FTS spectrograph at the Mayall telescope), one of the brightest stars on the Northern hemisphere. Thus it is well studied (see e.g. Griffin & Griffin 1967; McWilliam 1990; Ramírez et al. 2013, to mention just a few). We use the atlas from Hinkle et al. (2003) which covers the spectral range of interest (YJHK bands). Strong telluric features were identified with a spectrum from the TAPAS web page (Bertaux et al. 2014). The atlas also comes with a telluric standard and the ratio of the two spectra in order to correct for the tellurics. The telluric spectrum from TAPAS is only used for telluric line identification. We use both the telluric corrected and non-corrected spectrum.

The spectrum for 10 Leo is from the CRIRES-POP team (Nicholls et al. 2016). 10 Leo is very similar to Arcturus, which is also one reason this star was the first to be fully reduced by the CRIRES-POP team. The spectrum is divided into each band YJ (only together), H, K, L, and M. We use only the first three. Some small gaps are present in the spectrum due to tellurics that could not be properly removed, low S/N, bad pixels, etc. Rather than giving an uncertain interpolation, Nicholls et al. (2016) decided to leave small gaps in the data. This has very little effect on our line by line analysis. However, we were unable to measure one Fe II line due to the gaps, which are generally important to determine the surface gravity.

The data for the two stars are very similar in terms of S/N (around 300 as measured by IRAF in a continuum region in the YJ band), resolution (approximately 100 000), and spectral coverage. In Fig. 1 we compare the spectra of the two stars in a region with some of the iron lines used for the analysis described below.

3. Refining the NIR line list

In Paper I we prepared a Fe I and Fe II line list in the NIR domain. This line list was calibrated using a solar spectrum, and successfully used to derive atmospheric parameters for a late F star. Here we will go one step forward, and test this line list for K type stars. Besides testing the line list from Paper I at cooler effective temperatures with two K stars, it is a primary goal of this work to refine the line list. This includes identifying recurring outliers (both from the work done in Paper I and in this work), and lines which we are not able to measure, e.g. if a line is amidst a forest of telluric lines. To identify these lines the solar atlas used in Paper I was revisited. In total 211/295 Fe I lines and 8/13 Fe II lines were removed in the process. Most of these were blended lines with either tellurics or other stellar lines. This procedure leaves us with 84 Fe I lines and 5 Fe II lines. These lines should be the best for deploying our technique of determining atmospheric stellar parameters.

During a second look at the Solar spectrum, the EW of the lines were measured by hand (this had previously been done automatically with ARES). Since we re-measured the EWs, the log gf values had to be re-calibrated again. Here we simply change the log gf values for the measured EW until the abundance of a given line is equal to that of the Sun, using the same solar atmosphere model as in Paper I. The mean change in log gf for common lines is -0.09 ± 0.16. The line list with the updated log gf is presented in Appendix A.

The Fe II lines are used to determine $\log g$ by imposing ionization balance with the average Fe I abundance. However, the low number of Fe II lines available is a concern, since the average abundance of Fe II is affected more by small number statistics compared to the numerous Fe I lines.

4. Results

We derive the stellar atmospheric parameters in the same way as described in Paper I using the new minimization tool, FASMA (Andreasen et al. 2017). We use ATLAS9 atmosphere models during the derivation (Kurucz 1993). The EWs are measured for both stars automatically with ARES (Sousa et al. 2015) and by

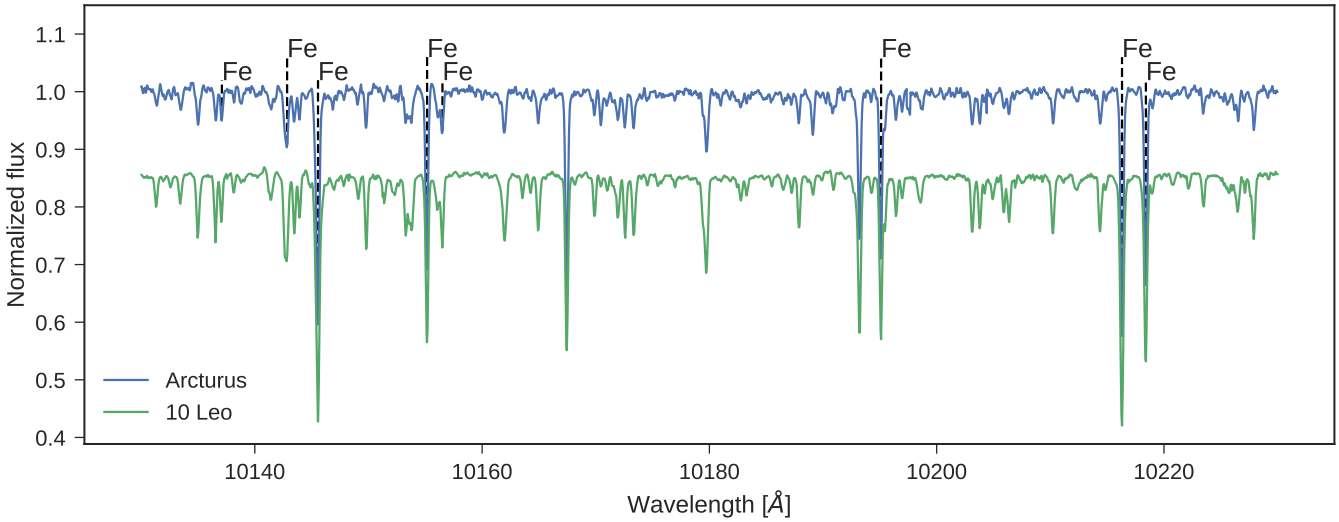

Fig. 1. Sample spectra of the two stars, in blue is Arcturus, and green is 10 Leo with an 0.15 offset. We mark the location of Fe I lines in the region.

hand with splot in IRAF. We compare the derived stellar parameters from the two measured sets of EWs, and with average adopted literature values.

4.1. Revisiting HD 20010

As a first step we revisit HD 20010 for which we derived atmospheric stellar parameters in Paper I using the newly revised line list presented in this paper. The results are presented in Tab. 1 along with the average literature values (see Paper I and references therein). We see better agreement with the average literature values adopted (especially [Fe/H] and $\log g$), and smaller errors with the updated results. This suggest that the new line list is more reliable.

4.2. Arcturus

Arcturus is one of the brightest stars on the night sky with a V magnitude of -0.05 (Ducati 2002). Hence it is a prime target for testing the updated line list with numerous measurements of the atmospheric parameters as mentioned above.

The atlas consists of both a summer observation set and a winter observation set. This is in order to minimize the effect of tellurics at different spectral regions. A comparison between the two sets of measured EWs - both the manual measurements using IRAF and the automatic measurements using ARES - are shown in Fig. 2. The automatic EW measurements for the summer set and winter set shows excellent agreement. This means that the two data sets are very similar, thus we chose to only manually measure the EWs for one set (summer). We did, however, measure a few lines from the winter data set to verify the agreement. For both the automatically and manually measured EWs, we discard all lines with an EW below 5 mÅ and above 150 mÅ before continuing the analysis. Lines outside this range are either too weak to be reliable measured or are so strong that the we are not able to fit a Gaussian to the profile. Especially the wings of the absorption lines are a problem for strong lines. For all three sets of measured EWs (summer and winter observations automatically, and summer manually), parameters were derived with and without $\log g$ set to a fixed value (1.69 dex, the average literature value adopted). The derivation of the parameters follow the procedure presented in Paper I. We use the minimization routine from Andreasen et al. (2017). After we reach convergence using all the iron lines we were able to measure, one outlier above 3σ in abundance were removed, and the minimization routine was restarted. This process was done iteratively until there were no more outliers. The final results are presented in Tab. 2 together with mean parameters from the literature.

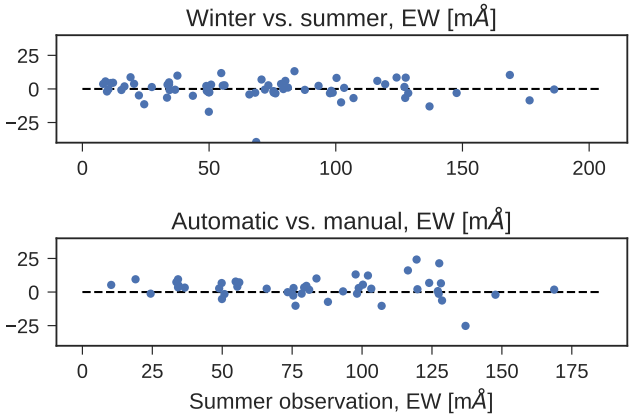

Fig. 2. Top figure: Difference of the automatic EW measurements between the summer observations and winter observations from the Arcturus spectra. Bottom figure: Same as above, but with manual measurements from ARES (summer) and automatic measurements (summer).

We generally see good agreement between the derived parameters and the average values from the literature adopted. The only parameter being difficult to measure is the surface gravity due to the low number of Fe II lines in the NIR. It is very important to derive the metallicity accurately, and we report good results overall, but especially with the automatic measurements, compared to literature values. When measuring the EWs by hand, we might have systematically overestimated the continuum, resulting in higher [Fe/H]. For visualization the parameters are plotted (except $\xi_{\rm micro}$) in Fig. 3. Here the histogram shows the literature values collected from Simbad while the ver-

Table 1. Updated results for HD 20010 using the shorter line list and new oscillator strengths.

	$T_{\rm eff}$ (K)	$\log g$ (dex)	$\xi_{\rm micro}$ (km/s)	[Fe/H] (dex)
Literature	6131 ± 255	4.01 ± 0.60	1.90 ± 1.08	−0.23 ± 0.14
This work	6157 ± 180	4.06 ± 0.76	1.62 ± 0.44	−0.18 ± 0.11
This work	6153 ± 176	4.01 (fixed)	1.68 ± 0.40	−0.18 ± 0.11
Paper I	6116 ± 224	4.21 ± 0.58	2.45 ± 0.45	−0.14 ± 0.14
Paper I	6144 ± 212	4.01 (fixed)	2.66 ± 0.42	−0.13 ± 0.29

Table 2. The derived parameters for Arcturus with and without fixed surface gravity. The literature values are a simple mean of all the available parameters on Simbad with the corresponding standard error. There is no microturbulence available, so we derived it using the empirical relation from Adibekyan et al. (2015) for each set of parameters.

	$T_{\rm eff}$ (K)	$\log g$ (dex)	$\xi_{\rm micro}$ (km/s)	[Fe/H] (dex)
Literature	4306 ± 100	1.69 ± 0.32	1.92 ± 0.15	−0.54 ± 0.11
IRAF	4380 ± 79	0.64 ± 0.33	1.14 ± 0.09	−0.49 ± 0.07
IRAF	4212 ± 77	1.69 (fixed)	1.25 ± 0.08	−0.37 ± 0.03
ARES (summer)	4439 ± 63	1.20 ± 0.20	1.55 ± 0.10	−0.58 ± 0.06
ARES (summer)	4348 ± 75	1.69 (fixed)	1.58 ± 0.09	−0.53 ± 0.03
ARES (winter)	4436 ± 67	0.55 ± 1.77	1.35 ± 0.09	−0.56 ± 0.07
ARES (winter)	4233 ± 109	1.69 (fixed)	1.43 ± 0.09	−0.49 ± 0.04
Weighted mean	4421 ± 40	0.96 ± 0.60	1.34 ± 0.05	−0.55 ± 0.04
Weighted mean	4269 ± 51	1.69 (fixed)	1.41 ± 0.05	−0.46 ± 0.02

tical black line is our final value with gray shaded errorbar. The plot shows that our values are in very good agreement with the literature results, supporting the quality and reliability of our analysis.

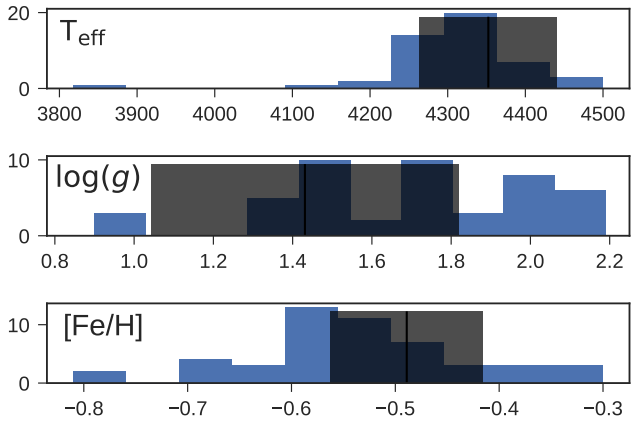

Fig. 3. Histogram of the different sets of literature parameters of Arcturus (except $\xi_{\rm micro}$). The black vertical line are our derived parameters, and the gray shaded area are the errors on the corresponding parameters.

4.3. 10 Leo

The approach for determining the atmospheric stellar parameters for 10 Leo is identical to Arcturus. We use ARES on each band (YJ, H, and K-band) separately. For the small gaps in the spectrum, we simply set the flux to 1, since the spectrum is already normalized. This will also prevent ARES to identify and measure any lines in these regions. The EWs from the three regions are combined to one final line list used for the determination of the parameters. The EWs were also measured by hand using IRAF. We list the results in Tab. 3 alongside with an average of literature values taken from Simbad. The final results and five collected literature values are presented in Fig. 4.

Generally the derived parameters are in excellent agreement with the literature values listed here. We were able to derive good $\log g$ values, although with larger errors compared to the results from the literature.

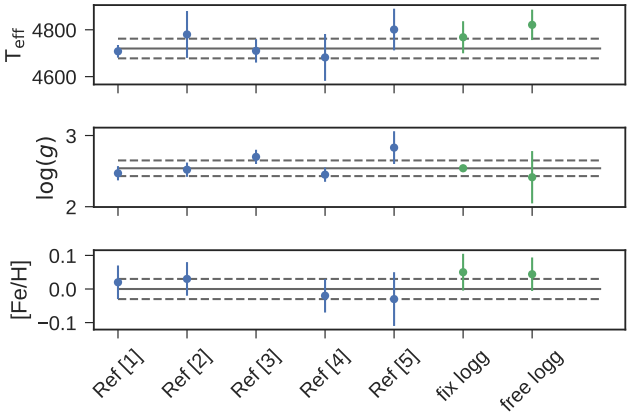

Fig. 4. Literature values (blue) and the two results from this work (green) with and without $\log g$ fixed. The errorbars on the literature values are either those presented in the corresponding paper, or in the cases none were presented we give an error of 100 K for $T_{\rm eff}$, 0.10 dex for $\log g$, and 0.05 dex for [Fe/H]. The horizontal lines are the average literature values adopted. References: Ref [1]: Luck (2015), Ref [2]: Park et al. (2013), Ref [3]: Massarotti et al. (2008), Ref [4]: Soubiran et al. (2008), and Ref [5]: da Silva et al. (2011).

5. Discussion

5.1. The role of $\log g$

One of the most difficult atmospheric stellar parameters to get from a spectrum is the surface gravity. For this we need the lines

Table 3. Results from 10 Leo presented in the same way as for Tab. 2.

	$T_{\rm eff}$ (K)	$\log g$ (dex)	$\xi_{\rm micro}$ (km/s)	[Fe/H] (dex)
Literature	4720 ± 42	2.54 ± 0.11	1.59 ± 0.02	0.00 ± 0.03
IRAF	4835 ± 85	2.41 ± 0.41	1.28 ± 0.08	0.09 ± 0.06
IRAF	4768 ± 88	2.54 (fixed)	1.20 ± 0.08	0.01 ± 0.05
ARES	4805 ± 98	2.42 ± 0.61	1.23 ± 0.10	−0.01 ± 0.07
ARES	4768 ± 105	2.54 (fixed)	1.20 ± 0.10	−0.01 ± 0.06
Weighted mean	4821 ± 65	2.41 ± 0.37	1.26 ± 0.06	0.04 ± 0.05
Weighted mean	4768 ± 69	2.54 (fixed)	1.20 ± 0.06	0.05 ± 0.04

of pressure sensitive ionized atoms such as Fe II. However, they are more sparse than neutral iron, Fe I, making the determination more challenging. This is true in the optical (see e.g. the discussion by Mortier et al. 2013), and even more in the NIR (see e.g. Paper I). One solution to this problem is to fix the value of surface gravity and derive the other parameters. With the parallaxes from Gaia (Gaia Collaboration et al. 2016) we will have access to accurate $\log g$. However, this requires a prior knowledge of the mass from e.g. isochrones, and $T_{\rm eff}$. By iteratively obtaining the $T_{\rm eff}$ from spectroscopy and the corresponding $\log g$ from the parallaxes, we can obtain reliable $T_{\rm eff}$, $\log g$, and [Fe/H]. Without the final parallaxes from Gaia we may yet only rely on literature values for $\log g$. As seen from Fig. 3, the distribution of $\log g$ values from the literature are rather disperse. Since there is a dependence between the other derived parameters with $\log g$, simply using a mean value as a reference value can lead to misleading parameters. To verify the impact of using the wrong $\log g$ as baseline, we tested what was the $T_{\rm eff}$ and [Fe/H] that we derive by setting $\log g$ fixed to values between 0.9 dex and 2.2 dex, i.e., in the range of the literature values found. The results show that $T_{\rm eff}$ and [Fe/H] can change by 200 K and 0.21 dex, respectively. This is most likely the origin of the small discrepancies seen for the parameters of Arcturus when the $\log g$ is fixed and free.

Note that the ionized iron lines are not only sparse, they are also rather weak. The lowest measured EW for an Fe II line is 7.8 mÅ (in Arcturus), while the highest measured value is 20.7 mÅ (in 10 Leo). However, with the upcoming high quality spectra for the NIR, the community should still be able to measure these Fe II lines.

5.2. Proper data reduction

The relative novelty of NIR high resolution spectroscopy is reflected on a number of problems regarding the available spectra that made our analysis particularly difficult. For instance, in Paper I we had to deal with a less reliable wavelength calibration for the spectrum of HD 20010. This meant the wavelength was stretched when compared to a synthetic spectrum, which is discussed in more detail by Nicholls et al. (2016). The poor wavelength calibration for HD 20010 most likely caused bad EW measurements. In addition, the spectrum was not corrected for telluric lines which also caused minor deviation from the true EW when measured. Another reason was the non-refined line list used, which we have attempted to correct for here. The refined line list has made the derivation of the metallicity more reliable compared with the adopted literature as it is demonstrated in Sec. 4.1. It is expected that even better results will be obtained for this star once the final spectrum is presented by the CRIRES-POP team.

All the above problems we had with HD 20010 have been solved for 10 Leo, and it is clear the results are of much higher quality. This can be seen by the smaller errors we have on our parameters, and the good agreement of all parameters compared with the literature. Therefore, it may be needed that a telluric correction is applied to the spectrum before atmospheric stellar parameters can be determined reliably. However, with our limited sample it is hard to make a clear conclusion yet.

6. Conclusion

In this paper we present a refined Fe I and Fe II line list in the NIR domain. The method should work in all spectral ranges, however, it is important to locate the appropriate iron lines. For the NIR we need a relative large coverage (YJHK, although few lines are in the K band). The method used here which is usually adopted in the optical domain to derive parameters is now available for the NIR as well. The refined line list has been used to derive new parameters for the late F-star HD 20010, as well as for two K-giants (Arcturus and 10 Leo). The results show that the stellar atmospheric parameters derived using our line list are perfectly compatible with the literature values. We are thus now extending the line list towards cooler temperatures. With the updated results for HD 20010, and the results for Arcturus and 10 Leo, we are now reaching the same precision that has been reached in the optical for similar spectral types using the same methodology. The obvious next step is to approach the even cooler M stars. Particular interesting are the M dwarf stars, known to be prone forming rocky planets. As important as cooler stars, we have yet to test our line list on any dwarf stars other than the Sun for which our line list is calibrated. The upcoming spectral library from CARMENES (priv. comm. with P. Amado) will provide the community with high quality spectra and allow us to extend our test to many different spectral types of interest.

Acknowledgements. We thank José Caballero for many useful for comments during the process which led to this paper. He has been most kind providing help whenever needed. This work was supported by Fundação para a Ciência e a Tecnologia, FCT, (ref. UID/FIS/04434/2013, PTDC/FIS-AST/1526/2014, and PTDC/FIS-AST/7073/2014) through national funds and by FEDER through COMPETE2020 (ref. POCI-01-0145-FEDER-007672, POCI-01-0145-FEDER-016886, and POCI-01-0145-FEDER-016880). N.C.S., and S.G.S. acknowledge the support from FCT through Investigador FCT contracts of reference IF/00169/2012, and IF/00028/2014, respectively, and POPH/FSE (EC) by FEDER funding through the program "Programa Operacional de Factores de Competitividade - COMPETE". E.D.M acknowledge the support from the FCT in the form of the grants SFRH/BPD/76606/2011. This research has made use of the SIMBAD database operated at CDS, Strasbourg (France).

References

Adibekyan, V. Z., Benamati, L., Santos, N. C., et al. 2015, MNRAS, 450, 1900
Ammler-von Eiff, M., Santos, N. C., Sousa, S. G., et al. 2009, A&A, 507, 523
Andreasen, D. T., Sousa, S. G., Delgado Mena, E., et al. 2016, A&A, 585, A143
Andreasen, D. T., Sousa, S. G., Tsantaki, M., et al. 2017, A&A, 585, A143
Artigau, É., Kouach, D., Donati, J.-F., et al. 2014, in Society of Photo-Optical Instrumentation Engineers (SPIE) Conference Series, Vol. 9147, Society of Photo-Optical Instrumentation Engineers (SPIE) Conference Series, 15

Baraffe, I., Homeier, D., Allard, F., & Chabrier, G. 2015, A&A, 577, A42
Bensby, T., Feltzing, S., & Oey, M. S. 2014, A&A, 562, A71
Bertaux, J. L., Lallement, R., Ferron, S., Boonne, C., & Bodichon, R. 2014, A&A, 564, A46
Blackwell, D. E. & Shallis, M. J. 1977, MNRAS, 180, 177
Boyajian, T. S., von Braun, K., van Belle, G., et al. 2012, ApJ, 757, 112
Casagrande, L., Ramírez, I., Meléndez, J., Bessell, M., & Asplund, M. 2010, A&A, 512, A54
Conod, U., Blind, N., Wildi, F., & Pepe, F. 2016, in Proc. SPIE, Vol. 9909, Society of Photo-Optical Instrumentation Engineers (SPIE) Conference Series, 990941
da Silva, R., Milone, A. C., & Reddy, B. E. 2011, A&A, 526, A71
Delfosse, X., Donati, J.-F., Kouach, D., et al. 2013, in SF2A-2013: Proceedings of the Annual meeting of the French Society of Astronomy and Astrophysics, ed. L. Cambresy, F. Martins, E. Nuss, & A. Palacios, 497–508
Dotter, A., Chaboyer, B., Jevremović, D., et al. 2008, ApJS, 178, 89
Ducati, J. R. 2002, VizieR Online Data Catalog, 2237
Follert, R., Dorn, R. J., Oliva, E., et al. 2014, in Society of Photo-Optical Instrumentation Engineers (SPIE) Conference Series, Vol. 9147, Society of Photo-Optical Instrumentation Engineers (SPIE) Conference Series, 19
Gaia Collaboration, Prusti, T., de Bruijne, J. H. J., et al. 2016, A&A, 595, A1
Girardi, L., Bressan, A., Bertelli, G., & Chiosi, C. 2000, A&A Supp., 141, 371
Griffin, R. & Griffin, R. 1967, MNRAS, 137, 253
Hinkle, K., Wallace, L., Livingston, W., et al. 2003, in Cambridge Workshop on Cool Stars, Stellar Systems, and the Sun, Vol. 12, The Future of Cool-Star Astrophysics: 12th Cambridge Workshop on Cool Stars, Stellar Systems, and the Sun, ed. A. Brown, G. M. Harper, & T. R. Ayres, 851–856
Kjeldsen, H. & Bedding, T. R. 1995, A&A, 293, 87
Kotani, T., Tamura, M., Suto, H., et al. 2014, in Society of Photo-Optical Instrumentation Engineers (SPIE) Conference Series, Vol. 9147, Society of Photo-Optical Instrumentation Engineers (SPIE) Conference Series, 14
Kurucz, R. 1993, ATLAS9 Stellar Atmosphere Programs and 2 km/s grid. Kurucz CD-ROM No. 13. Cambridge, Mass.: Smithsonian Astrophysical Observatory, 1993., 13
Lebzelter, T., Heiter, U., Abia, C., et al. 2012, A&A, 547, A108
Lindgren, S., Heiter, U., & Seifahrt, A. 2016, A&A, 586, A100
Luck, R. E. 2015, AJ, 150, 88
Massarotti, A., Latham, D. W., Stefanik, R. P., & Fogel, J. 2008, AJ, 135, 209
McWilliam, A. 1990, ApJS, 74, 1075
Meléndez, J. & Barbuy, B. 1999, ApJS, 124, 527
Mortier, A., Santos, N. C., Sousa, S. G., et al. 2013, A&A, 558, A106
Mucciarelli, A., Pancino, E., Lovisi, L., Ferraro, F. R., & Lapenna, E. 2013, ApJ, 766, 78
Nicholls, C. P., Lebzelter, T., Smette, A., et al. 2016, ArXiv e-prints [e-prints[arXiv]1609.07873]
Önehag, A., Heiter, U., Gustafsson, B., et al. 2012, A&A, 542, A33
Origlia, L., Oliva, E., Baffa, C., et al. 2014, in Society of Photo-Optical Instrumentation Engineers (SPIE) Conference Series, Vol. 9147, Society of Photo-Optical Instrumentation Engineers (SPIE) Conference Series, 1
Park, S., Kang, W., Lee, J.-E., & Lee, S.-G. 2013, AJ, 146, 73
Quirrenbach, A., Amado, P. J., Caballero, J. A., et al. 2014, in Society of Photo-Optical Instrumentation Engineers (SPIE) Conference Series, Vol. 9147, Society of Photo-Optical Instrumentation Engineers (SPIE) Conference Series, 1
Ramírez, I., Allende Prieto, C., & Lambert, D. L. 2013, ApJ, 764, 78
Ramírez, I. & Meléndez, J. 2005, ApJ, 626, 446
Rayner, J., Bond, T., Bonnet, M., et al. 2012, in Proc. SPIE, Vol. 8446, Ground-based and Airborne Instrumentation for Astronomy IV, 84462C
Rayner, J., Tokunaga, A., Jaffe, D., et al. 2016, in Proc. SPIE, Vol. 9908, Society of Photo-Optical Instrumentation Engineers (SPIE) Conference Series, 990884
Recio-Blanco, A., Bijaoui, A., & de Laverny, P. 2006, MNRAS, 370, 141
Santos, N. C., Sousa, S. G., Mortier, A., et al. 2013, A&A, 556, A150
Soubiran, C., Bienaymé, O., Mishenina, T. V., & Kovtyukh, V. V. 2008, A&A, 480, 91
Sousa, S. G., Santos, N. C., Adibekyan, V., Delgado-Mena, E., & Israelian, G. 2015, A&A, 577, A67
Sousa, S. G., Santos, N. C., Mayor, M., et al. 2008, A&A, 487, 373
Torres, G., Andersen, J., & Giménez, A. 2010, A&A Rev., 18, 67
Torres, G., Fischer, D. A., Sozzetti, A., et al. 2012, ApJ, 757, 161
Torres, G., Winn, J. N., & Holman, M. J. 2008, ApJ, 677, 1324
Tsantaki, M., Sousa, S. G., Adibekyan, V. Z., et al. 2013, A&A, 555, A150
Tsantaki, M., Sousa, S. G., Santos, N. C., et al. 2014, A&A, 570, A80
Valenti, J. A. & Fischer, D. A. 2005, ApJS, 159, 141

Appendix A: Complete refined line list

The complete refined line list with Solar EWs measured by hand using IRAF.

Table A.1. Refined line list with all Fe I and Fe II lines and corresponding atomic data, including the updated oscillator strengths. This table is available online.

Wavelength (Å)	Element	EP (eV)	log gf	Solar EW (mÅ)
10065.05	Fe I	4.83	-0.279	94.0
10080.42	Fe I	5.10	-1.964	5.9
10081.39	Fe I	2.42	-4.512	6.9
10086.24	Fe I	2.95	-3.978	7.0
10137.10	Fe I	5.09	-1.736	9.8
10142.84	Fe I	5.06	-1.554	14.9
10145.56	Fe I	4.80	-0.118	109.0
10155.16	Fe I	2.18	-4.336	16.2
10156.51	Fe I	4.59	-2.109	12.2
10167.47	Fe I	2.20	-2.319	125.7
10195.11	Fe I	2.73	-3.608	22.6
10216.31	Fe I	4.73	0.047	129.9
10218.41	Fe I	3.07	-2.893	40.9
10265.22	Fe I	2.22	-4.648	8.1
10307.45	Fe I	4.59	-2.432	6.4
10332.33	Fe I	3.63	-3.131	10.5
10340.89	Fe I	2.20	-3.665	46.6
10347.97	Fe I	5.39	-0.717	37.0
10353.81	Fe I	5.39	-0.989	24.2
10364.06	Fe I	5.45	-1.100	18.0
10379.00	Fe I	2.22	-4.236	18.7
10388.75	Fe I	5.45	-1.471	8.7
10395.80	Fe I	2.18	-3.435	61.3
10423.03	Fe I	2.69	-3.658	22.9
10423.74	Fe I	3.07	-3.119	29.9
10469.65	Fe I	3.88	-1.277	89.3
10532.24	Fe I	3.93	-1.650	64.4
10555.65	Fe I	5.45	-1.282	13.1
10577.14	Fe I	3.30	-3.222	17.2
10616.72	Fe I	3.27	-3.306	15.6
10725.19	Fe I	3.64	-2.948	15.7
10753.00	Fe I	3.96	-2.077	39.7
10780.69	Fe I	3.24	-3.553	10.4
10783.05	Fe I	3.11	-2.786	47.0
10818.28	Fe I	3.96	-2.160	35.6
10863.52	Fe I	4.73	-0.877	67.1
10884.26	Fe I	3.93	-2.129	39.1
10896.30	Fe I	3.07	-2.911	42.9
11013.24	Fe I	4.80	-1.240	42.4
11026.79	Fe I	3.94	-2.517	21.2
11119.80	Fe I	2.85	-2.452	84.8
11641.80	Fe I	4.58	-2.116	15.6
11778.42	Fe I	5.34	-1.708	8.4
12053.08	Fe I	4.56	-1.602	41.3
12119.50	Fe I	4.59	-1.897	25.0
12213.34	Fe I	4.64	-2.006	19.1
12227.11	Fe I	4.61	-1.408	51.5
12244.92	Fe I	3.64	-3.222	11.8
12340.48	Fe I	2.28	-4.680	9.4
12342.92	Fe I	4.64	-1.545	42.1
12510.52	Fe I	4.96	-1.930	12.9
12557.00	Fe I	2.28	-4.026	33.8
12615.93	Fe I	4.64	-1.686	35.7
12638.70	Fe I	4.56	-0.679	112.3
12807.15	Fe I	3.64	-2.649	37.1
12808.24	Fe I	4.99	-1.811	16.4
12824.86	Fe I	3.02	-3.612	20.1
12840.57	Fe I	4.96	-1.612	25.3
12879.77	Fe I	2.28	-3.525	68.7
12896.12	Fe I	4.91	-1.713	23.2

Table A.1. continued.

Wavelength (Å)	Element	EP (eV)	log gf	Solar EW (mÅ)
12933.01	Fe I	5.02	-1.879	13.9
12934.67	Fe I	5.39	-1.103	30.9
13014.84	Fe I	5.45	-1.542	12.3
13352.17	Fe I	5.31	-0.355	94.4
13392.10	Fe I	5.35	-0.105	115.1
15194.49	Fe I	2.22	-4.808	14.1
15201.57	Fe I	5.49	-1.315	29.0
15207.53	Fe I	5.38	0.311	215.9
15335.38	Fe I	5.41	0.252	205.2
15490.34	Fe I	2.20	-4.787	16.1
15593.74	Fe I	5.03	-1.796	28.0
15611.15	Fe I	3.42	-2.966	51.6
15631.95	Fe I	5.35	0.171	207.0
15648.51	Fe I	5.43	-0.633	93.8
15676.58	Fe I	5.11	-1.848	22.3
16198.50	Fe I	5.41	-0.376	131.4
17420.83	Fe I	3.88	-3.628	6.7
19923.34	Fe I	5.02	-1.536	49.7
21851.38	Fe I	3.64	-3.578	12.7
22257.11	Fe I	5.06	-0.704	132.5
22380.80	Fe I	5.03	-0.377	179.4
22392.88	Fe I	5.10	-1.330	60.8
22619.84	Fe I	4.99	-0.564	158.2
23308.48	Fe I	4.08	-2.705	31.3
10427.31	Fe II	6.08	-1.575	13.7
10501.50	Fe II	5.55	-1.861	19.5
10862.64	Fe II	5.59	-2.006	15.3
11125.58	Fe II	5.62	-2.213	10.5
13251.14	Fe II	9.41	0.768	13.4